Fusion Engineering and Design 123 (2017) 513–517

Contents lists available at ScienceDirect

Fusion Engineering and Design

journal homepage: www.elsevier.com/locate/fusengdes

Optimal current profile control for enhanced repeatability of L-mode and H-mode discharges in DIII-D

William Wehner[a,*], Justin Barton[a], Menno Lauret[a], Eugenio Schuster[a], John R. Ferron[b], Chris Holcomb[c], Tim C. Luce[b], David A. Humphreys[b], Michael L. Walker[b], Ben G. Penaflor[b], Robert D. Johnson[b]

[a] Department of Mechanical Engineering and Mechanics, Lehigh University, Bethlehem, PA 18015, USA
[b] General Atomics, San Diego, CA 92121, USA
[c] Lawrence Livermore National Laboratory, Livermore, CA 94550, USA

HIGHLIGHTS

- Model-based current profile control for reproducibility of target current profiles.
- Control-oriented modeling, optimal feedforward control, and linearized feedback.
- Experimental validation in both L-mode and H-mode DIII-D discharges.

ARTICLE INFO

Article history:
Received 3 October 2016
Received in revised form 1 March 2017
Accepted 5 March 2017
Available online 27 March 2017

Keywords:
Current profile control
Safety factor profile control
Optimal control
Optimal plasma scenario planning

ABSTRACT

In this work, model-based control techniques are used to obtain target current profiles in low-confinement-mode (L-mode) as well as high-confinement-mode (H-mode) DIII-D discharges. The control problem is formulated as a trajectory optimization problem to search for a feasible path from the expected initial condition to the desired target. The result comprises a sequence of feedforward (open-loop) control requests and a corresponding state evolution from the initial condition to the desired target. On top of this optimal feedforward control sequence a feedback (closed-loop) controller based on a linearized model and optimal control design techniques is added to track the desired state evolution. The effectiveness of the control approach is demonstrated with experiments.

1. Introduction

Serious interest in active current profile control is rapidly growing in the tokamak research community. This is because elements of a high quality plasma such as long energy confinement time, stability against deleterious magneto-hydro-dynamic (MHD) [1] activity, access to steady state scenarios [2] and potential for high fusion gain [3] are all closely linked to the current profile distribution. Presently, tokamak operation typically relies on "scenario planning", i.e. preprogramming a set of auxiliary current drive and heating powers according to semi-empirical laws to obtain a desired operating scenario. In this work we follow a model based control approach combining both feedforward and feedback control techniques, which effectively automates the scenario planning task, in an attempt to improve shot-to-shot reproducibility of target current profiles (equivalently target q profiles).

The evolution of the current profile is closely related to the evolution of the poloidal magnetic flux profile, which can be properly modeled in a first-principles manner by a nonlinear partial differential equation (PDE) referred to as the magnetic flux diffusion equation (MDE) [4]. Simplified, control-oriented formulations of the MDE have already been developed for the DIII-D tokamak for both L-mode [5] and H-mode discharges [6]. In both cases, the control-oriented models combine the MDE with physics-based correlations for the electron temperature, plasma resistivity, and non-inductive current drive sources including neutral beam injection (NBI), electron cyclotron current drive (ECCD), and bootstrap current drive.

The control objective is to reach a specified target profile shape at a specified time. To accomplish this, first, an open-loop control problem is formulated as a trajectory optimization problem to find a feasible path from the expected initial condition to the desired

* Corresponding author.
E-mail address: wehner@lehigh.edu (W. Wehner).

http://dx.doi.org/10.1016/j.fusengdes.2017.03.022
0920-3796/

target. The problem involves the minimization of a scalar objective over a set of constraints associated with the dynamics of the system (model of the q profile evolution), actuator constraints (physical limits such as maximum NBI power), and bounds on the acceptable current profile shape through the ramp-up phase. Finally, we combine the feedforward control approach with feedback control to compensate for model mismatches between the physical system and the approximate control-oriented model as well as for disturbances. Several approaches to current profile feedback control have been explored such as passivity-based control [7,8], H_∞ control [9], optimal control [10], and receding horizon control [11,12]. This work focuses on the feedforward control design. The feedback design based on linear quadratic optimization, chosen for simplicity of implementation, is formally detailed in [13].

The control-oriented modeling of the q profile evolution is briefly described in Section 2, details of the feedforward and feedback control design approach are given in Section 3, experimental evidence of the effectiveness of the controller in reaching the target is presented in Section 4, and, finally, conclusions are made in Section 5.

2. Modeling the current profile evolution

The current density profile can be described as a function of the poloidal magnetic flux profile, $\psi(\hat{\rho}, t)$, whose dynamics can be well modeled by the MDE [4]. We can compactly model the evolution of ψ in response to the various actuators as

$$\frac{\partial \psi}{\partial t} = c_1 \frac{1}{\hat{\rho}} \frac{\partial}{\partial \hat{\rho}} \left(\hat{\rho} c_2 \frac{\partial \psi}{\partial \hat{\rho}} \right) + c_3 (j_{\text{aux}} + j_{\text{bs}}) \tag{1}$$

along with the boundary conditions $\left.\frac{\partial \psi}{\partial \hat{\rho}}\right|_{\hat{\rho}=0} = 0$, $\left.\frac{\partial \psi}{\partial \hat{\rho}}\right|_{\hat{\rho}=1} = c_4 I_p$, where t represents time and $\hat{\rho}$ is the normalized spatial coordinate. The coefficients c_1, c_2, c_3, c_4 are time and space dependent functions. I_p denotes the total plasma current. The terms j_{aux} and j_{bs} represent non-inductively driven current densities from auxiliary sources and the bootstrap effect, respectively (see [6] for a complete description of the model and terms). Different operating scenarios are modeled separately by configuring the model parameters appropriately, for example DIII-D discharges in L-mode [5] and H-mode [6].

The control inputs (actuators) associated with the model (1) include the powers of the auxiliary heating and current drive sources (ECCD and NBI), which are denoted as $P_{\text{EC},1}, \ldots, P_{\text{EC},n_{\text{EC}}}, P_{\text{NBI},1}, \ldots, P_{\text{NBI},n_{\text{NBI}}}$, the total plasma current, and the line-averaged electron density $\bar{n}_e$. The system outputs of interest are the q profile and β_N (normalized β), $q \propto -\frac{B_{\phi,0}\rho_b^2 \hat{\rho}}{\partial \psi / \partial \hat{\rho}}$, $\beta_N \propto \frac{E}{B_{\phi,0} I_p}$, where $B_{\phi,0}$ is the vacuum toroidal magnetic field at the major radius, and E is the plasma stored energy.

To transform the model (1) to state-space form, we discretize the system (1) in space using finite difference approximations to the spatial derivatives. The domain of interest, $\hat{\rho} = [0, 1]$, is truncated to l evenly spaced nodes, separated by $\Delta\hat{\rho} = 1/(l-1)$ to obtain the finite-dimensional, nonlinear state-space system,

$$\dot{\mathbf{x}} = \boldsymbol{f}(\mathbf{x}, \mathbf{u}), \quad \mathbf{y} = \mathbf{h}(\mathbf{x}), \tag{2}$$

where the model state is $\mathbf{x} = [\psi_{\hat{\rho}=0.05}, \psi_{\hat{\rho}=0.1}, \ldots, \psi_{\hat{\rho}=0.95}, E]^T$, and the system output include the q profile at various $\hat{\rho}$ locations, $\boldsymbol{q} = [q_{\hat{\rho}=0.05}, q_{\hat{\rho}=0.01}, \ldots, q_{\hat{\rho}=.95}]^T$, and β_N ($\mathbf{y} = [\boldsymbol{q}^T, \beta_N]^T$). The input, $\mathbf{u}$, includes the actuators previously mentioned, i.e. $\mathbf{u} = [I_p, \bar{n}_e, P_{\text{EC},1}, \ldots, P_{\text{EC},n_{\text{EC}}}, P_{\text{NBI},1}, \ldots, P_{\text{NBI},n_{\text{NBI}}}]^T$.

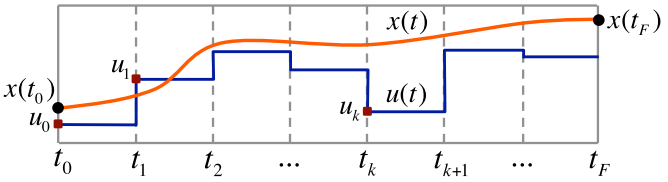

Fig. 1. Discretized control sequence, $\mathbf{u}(t \in [t_k, t_{k+1}]) = \mathbf{u}_k$, and output of integrator function $\mathbf{F}$, which maps $\mathbf{w} = [\mathbf{u}_0, \mathbf{u}_1, \ldots, \mathbf{u}_F]$, $\mathbf{x}_0$, and t to $\mathbf{x}(t)$.

3. Feedforward control via trajectory optimization

We formulate the feedforward control (pre-programmed control sequence) design as an optimization problem of the form

$$\begin{aligned} \underset{\mathbf{u}(t)}{\text{minimize}} \quad & J(\mathbf{x}(t_F)) \\ \text{subject to} \quad & \dot{\mathbf{x}} = \boldsymbol{f}(\mathbf{x}, \mathbf{u}), \\ & \mathbf{x}(t_0) = \mathbf{x}_0, \\ & \mathbf{g}_{\text{in}}(\mathbf{x}(t), \mathbf{u}(t)) \le 0, \\ & \mathbf{g}_{\text{eq}}(\mathbf{x}(t), \mathbf{u}(t)) = 0. \end{aligned} \tag{3}$$

This is often called a trajectory optimization problem because it involves the search for a state trajectory, $\mathbf{x}(t)$, that starts from the initial state, $\mathbf{x}_0$, and reaches some goal state at time t_F quantified by the scalar function J. This state trajectory must be consistent with the system dynamics described by the equality constraint $\dot{\mathbf{x}} = \boldsymbol{f}(\mathbf{x}, \mathbf{u})$. Additionally, the optimization requires the state trajectory to avoid undesirable regions of the state space, which are quantified by the constraints, $\mathbf{g}_{\text{in}}$ and $\mathbf{g}_{\text{eq}}$. The undesirable regions of the state space are those regions of the tokamak operating space that are associated with MHD instabilities.

The most successful approach to solving an optimal control problem like (3) is to parameterize the problem with a finite set of decision variables, and then to solve it by using numerical optimization methods [14]. As illustrated in Fig. 1, over a time grid $t_0, \ldots, t_F$, we discretize the control as a zero order hold, $\mathbf{u}(t \in [t_k, t_{k+1}]) = \mathbf{u}_k$, and then we prescribe $\mathbf{x}$ as a function of $\mathbf{w} = [\mathbf{u}_0, \mathbf{u}_1, \ldots, \mathbf{u}_F]$, $\mathbf{x}_0$, and t to obtain

$$\mathbf{x}(t) = \mathbf{F}(\mathbf{w}, \mathbf{x}_0, t) \equiv \mathbf{x}_0 + \int_{t_0}^{t} \boldsymbol{f}(\mathbf{x}(s), \mathbf{u}(s))\, ds. \tag{4}$$

The function $\mathbf{F}$ is an integrator function which depends on the choice of integration scheme used to simulate the system modeled by (2). With the use of (4), we can rewrite the original optimal control problem (3) as

$$\begin{aligned} \underset{\mathbf{w}}{\text{minimize}} \quad & J(\mathbf{F}(\mathbf{w}, \mathbf{x}_0, t_F)) \\ \text{subject to} \quad & \mathbf{g}_{\text{in}}(\mathbf{F}(\mathbf{w}, \mathbf{x}_0, t_i), \mathbf{u}_i) \le 0, \quad \text{for} \quad i = 0, 1, \ldots, F \\ & \mathbf{g}_{\text{eq}}(\mathbf{F}(\mathbf{w}, \mathbf{x}_0, t_i), \mathbf{u}_i) = 0, \quad \text{for} \quad i = 0, 1, \ldots, F \end{aligned} \tag{5}$$

where we are now optimizing over a finite set of optimization variables defined by the feedforward control sequence $\mathbf{w}$. Additionally, the constraints have been reduced to a finite number by evaluating $\mathbf{g}_{\text{eq}}$ and $\mathbf{g}_{\text{in}}$ only at the times t_i, for $i = 0, 1, \ldots F$.

First-order necessary conditions for optimality require solutions to the problem (5) to be feasible, i.e. to satisfy all the constraints, and to be a stationary point to the Lagrangian. By assuming for the moment that problem (5) includes only equality constraints, the Lagrangian can be written as $\mathcal{L} = J(\mathbf{w}) - \boldsymbol{\lambda}^T \mathbf{g}_{\text{eq}}(\mathbf{w})$, where $\boldsymbol{\lambda}$ is a Lagrange multiplier, and the first-order necessary conditions can be summarized as

$$\begin{bmatrix} \nabla J(\mathbf{w}) - \nabla \mathbf{g}_{\text{eq}}(\mathbf{w}) \boldsymbol{\lambda} \\ \mathbf{g}_{\text{eq}}(\mathbf{w}) \end{bmatrix} = 0, \tag{6}$$

where ∇ represents $\partial/\partial\mathbf{w}$. We can proceed to search for a minimizer to the problem (5) by searching for points that satisfy (6). The natural approach is to solve the nonlinear equations (6) with Newton's method. Start with an initial guess, $(\mathbf{w}_k, \boldsymbol{\lambda}_k)$, of the optimal solution, $(\mathbf{w}^\star, \boldsymbol{\lambda}^\star)$, and make updates $(\mathbf{w}_{k+1}, \boldsymbol{\lambda}_{k+1}) = (\mathbf{w}_k, \boldsymbol{\lambda}_k) + (\Delta\mathbf{w}_k, \Delta\boldsymbol{\lambda}_k)$, where the update, $(\Delta\mathbf{w}_k, \Delta\boldsymbol{\lambda}_k)$ is determined by solving a linear approximation of (6), i.e. it is given by the Newton step,

$$\begin{bmatrix} \nabla^2_{\mathbf{ww}}\mathcal{L}(\mathbf{w}_k) & -\nabla\mathbf{g}_{\text{eq}}(\mathbf{w}_k) \\ \nabla\mathbf{g}_{\text{eq}}(\mathbf{w}_k)^T & 0 \end{bmatrix} \begin{bmatrix} \Delta\mathbf{w}_k \\ \Delta\boldsymbol{\lambda}_k \end{bmatrix} = \begin{bmatrix} -\nabla J(\mathbf{w}_k) + \nabla\mathbf{g}_{\text{eq}}(\mathbf{w}_k)\boldsymbol{\lambda}_k \\ -\mathbf{g}_{\text{eq}}(\mathbf{w}_k) \end{bmatrix}. \tag{7}$$

Sequential quadratic programming (SQP), the numerical optimization method used in this work, reformulates (7) as a quadratic optimization problem (quadratic program (QP))

$$\begin{aligned} \underset{\Delta\mathbf{w}_k}{\text{minimize}} \quad & J(\mathbf{w}_k) + \nabla J(\mathbf{w}_k)^T \Delta\mathbf{w}_k + \frac{1}{2}\Delta\mathbf{w}_k^T(\nabla^2_{\mathbf{ww}}\mathcal{L})\Delta\mathbf{w}_k, \\ \text{subject to} \quad & \mathbf{g}_{\text{eq}}(\mathbf{w}_k) + \nabla\mathbf{g}_{\text{eq}}{}^T(\mathbf{w}_k)\Delta\mathbf{w}_k = 0. \end{aligned} \tag{8}$$

It can be shown that the solution of (8) is also given by (7) [15]. While it is not possible to include inequality constraints into Newton's method because the optimality conditions associated with inequality constraints are non-smooth, they can be incorporated into (8) in the same form as the equality constraints.

Several techniques can be applied to find the gradients ∇J, $\nabla\mathbf{g}_{\text{eq}}$, and $\nabla\mathbf{g}_{\text{in}}$, which include forward finite differences, forward sensitivity propagation, and the adjoint method (see [16] for a review of each one of them). Forward sensitivity propagation involves propagating the sensitivity of the state along the trajectory to changes in each of the optimization variables. In order to carry out this method, first we need to decide on a discrete integration scheme to approximate the evolution of the system modeled by (2). Because the dynamic model (1) is approximately a linear diffusion equation, an appropriate integration method is the backward Euler method,

$$\mathbf{x}_{k+1} = \mathbf{x}_k + dt\,\boldsymbol{f}(\mathbf{x}_{k+1}, \mathbf{u}_{k+1}). \tag{9}$$

We require an implicit integration scheme as in (9) to handle the stiffness associated with (1), which arises due to the steep changes in the coefficient profiles around the boundary. The sensitivity of the state with respect to the optimization variables, $\mathbf{w}$, can be computed during the "forward simulation" of the dynamics. Taking partial derivatives of (9) with respect to $\mathbf{w}$, we obtain

$$\frac{\partial\mathbf{x}_{k+1}}{\partial\mathbf{w}} = \frac{\partial\mathbf{x}_k}{\partial\mathbf{w}} + dt\left(\left.\frac{\partial\boldsymbol{f}}{\partial\mathbf{x}}\right|_{\substack{\mathbf{x}_{k+1} \\ \mathbf{u}_{k+1}}} \frac{\partial\mathbf{x}_{k+1}}{\partial\mathbf{w}} + \left.\frac{\partial\boldsymbol{f}}{\partial\mathbf{u}}\right|_{\substack{\mathbf{x}_{k+1} \\ \mathbf{u}_{k+1}}} \frac{\partial\mathbf{u}_{k+1}}{\partial\mathbf{w}}\right). \tag{10}$$

Since the optimization variables include only the control values we have $\partial\mathbf{x}_0/\partial\mathbf{w} = 0$, $\partial\mathbf{u}_0/\partial\mathbf{w} = [\mathbf{I}, \mathbf{0}, \ldots, \mathbf{0}]$, $\partial\mathbf{u}_1/\partial\mathbf{w} = [\mathbf{0}, \mathbf{I}, \ldots, \mathbf{0}]$, etc. From (4), it can be seen that $\partial\mathbf{F}(\mathbf{w}, \mathbf{x}_0, t_k)/\partial\mathbf{w} = \partial\mathbf{x}_{k+1}/\partial\mathbf{w}$, which can be used in the chain rule to obtain gradients of both the cost function and each of the constraints. For example,

$$\nabla J = \frac{\partial J}{\partial\mathbf{w}} = \frac{\partial J}{\partial\mathbf{F}(\mathbf{w}, \mathbf{x}_0, t_F)} \frac{\partial\mathbf{F}(\mathbf{w}, \mathbf{x}_0, t_F)}{\partial\mathbf{w}} = \frac{\partial J}{\partial\mathbf{x}_{t_F}} \frac{\partial\mathbf{x}_{t_F}}{\partial\mathbf{w}}, \tag{11}$$

where $\mathbf{x}_{t_F}$ is found by propagating (10) forward.

3.1. Cost function and constraints

The cost function J consists in this case of a weighted sum of objectives associated with reaching the target q profile, the target β_N value, and a measure of stationarity,

$$J = \|\boldsymbol{q}(t_F) - \boldsymbol{q}^t\|_{\mathbf{W}_q} + W_{\beta_N}(\beta_N(t_F) - \beta_N^t)^2 + \|\mathbf{g}_{\text{ss}}(t_F)\|_{\mathbf{W}_{\text{ss}}}, \tag{12}$$

where $\boldsymbol{q}^t$ represents the target q profile, β_N^t represents the target β_N value, and the terms $\mathbf{W}_q, W_{\beta_N}$ and $\mathbf{W}_{\text{ss}}$ are cost weights. The term $\mathbf{g}_{\text{ss}}$ represents the spatial derivative of the plasma loop voltage profile. The plasma stationarity is reached when the loop voltage profile is flat or equivalently when the spatial derivative is zero, i.e. $\mathbf{g}_{\text{ss}} = 0$.

The constraints include bounds and rate limits on the actuators, a limit on q, to avoid the onset of sawtooth oscillations, a limit on density associated with the Greenwald density limit, and an upper bound on β_N to avoid the onset of neoclassical tearing modes,

$$q > 1 + \epsilon, \quad \tilde{n}_e[10^{20}\,\text{m}^{-3}] \le \frac{I_p[\text{MA}]}{\pi a^2}, \quad \beta_N \le \beta_N^{\max}. \tag{13}$$

Prior experiments showed that the L-to-H transition power scaled approximately with the line-averaged electron density according to $P_{\text{LH}} = 2\tilde{n}_e^{3/4}$. Therefore, for the L-mode discharges we also include an additional constraint on total auxiliary injected power to avoid the possibility of transitioning from L-mode to H-mode.

The cost function (12) and each of the constraints (13) can be written as a function of the state $\mathbf{x}$ and control $\mathbf{u}$, therefore the gradients ∇J, $\nabla\mathbf{g}_{\text{in}}$, and $\nabla\mathbf{g}_{\text{eq}}$, can be obtained with the forward sensitivity propagation method described above.

3.2. Parameterizing the input function

The optimization problem as described above involves a set of optimization variables which includes the control variables at each time step k. This amounts to substantially large number of optimization variables making the problem difficult to solve. To reduce the complexity, sacrificing optimality to some extent, we choose to parameterize the control sequence $\mathbf{w}$ as a piecewise linear function, as illustrated in Fig. 2. Thus the optimization variables $\mathbf{w}$ are reduced to the set $\mathbf{p} = [\mathbf{p}_0, \mathbf{p}_1, \ldots, \mathbf{p}_5]$, which has dimension $6\times$ (# of actuators considered for optimization).

3.3. Feedback control design

Let us label the resulting optimal feedforward control as $\mathbf{u}_{\text{FF}}(t)$ and the corresponding state trajectory $\mathbf{x}_{\text{FF}}(t)$ as prescribed by the dynamic model (1). The feedback control design proceeds by first linearizing the model (1) around the feedforward trajectory at the target time (t_F) to obtain the linear model, $\dot{\tilde{\theta}} = \mathbf{A}\tilde{\theta} + \mathbf{B}\tilde{\mathbf{u}}$, $\tilde{\iota} = \mathbf{C}\tilde{\theta}$. To simplify the feedback control design, we first differentiate the model (1) with respect to $\hat{\rho}$ to obtain a state equation for the newly introduced variable $\theta = \partial\psi/\partial\hat{\rho}$ and later introduce the term $\iota = 1/q$. The $\tilde{\cdot}$ over each variable designates deviations with respect to the optimal feedforward reference, i.e. $\tilde{\theta} = \theta - \theta_{\text{FF}}$, $\tilde{\iota} = \iota - \iota_{\text{FF}}$, and $\tilde{\mathbf{u}} = \mathbf{u} - \mathbf{u}_{\text{FF}}$. With the use of this model we can obtain a linear feedback controller that will act to eliminate disturbances from the feedforward state trajectory, i.e. it will regulate the system toward the feedforward state trajectory. This is an effective approach as long as the disturbances are sufficiently small. We make use of the linear state feedback control design approach as described in [13].

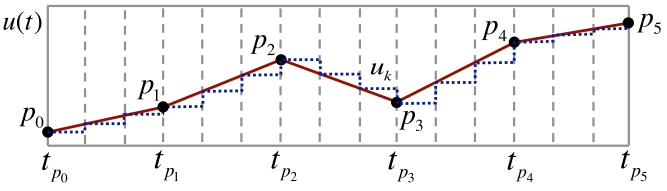

Fig. 2. Feedforward control is parameterized by a piecewise linear function parameterized by $\mathbf{p} = [p_0, p_1, p_2, \ldots, p_5]$.

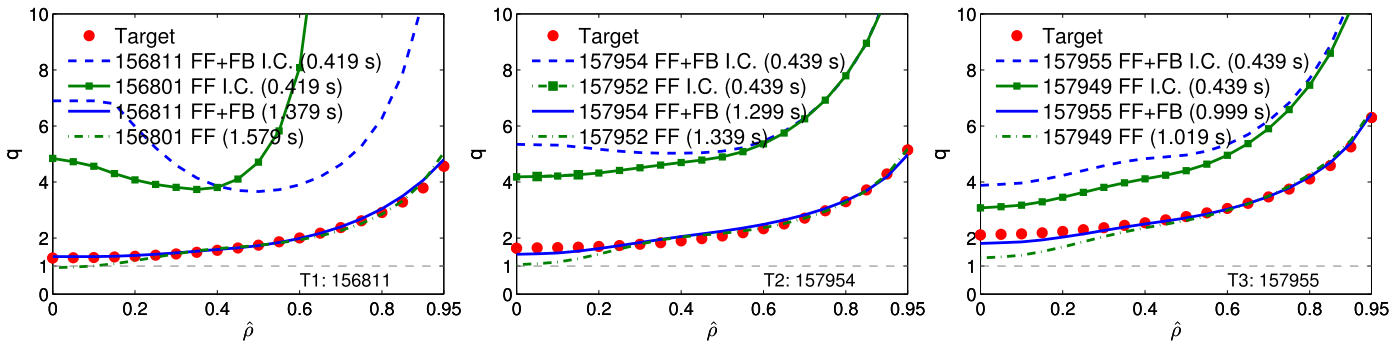

Fig. 3. Obtained q profiles for each of the three targets in L-mode discharges, Target 1 – $t_F = 1.0$ s (left), Target 2 – $t_F = 1.3$ s (middle), and Target 3 – $t_F = 1.5$ s (right). The red circles mark the target q profiles. Initial and final (best-matching) profiles are shown both for FF-only and FF + FB control shots. In each case, FF-only control shots are in green and FF + FB control shots are in blue. Generally, the initial conditions vary significantly from shot to shot. (For interpretation of the references to color in this figure legend, the reader is referred to the web version of the article.)

The end result is a controller of the form $\tilde{\mathbf{u}} = \mathbf{K}[\tilde{\theta}^T, \boldsymbol{\zeta}^T]^T$, where the gain matrix, $\mathbf{K}$, is obtained by minimizing the cost function

$$J_{\mathrm{FB}}(\mathbf{K}) = \int_0^\infty [\tilde{\imath}^T(t)\,\zeta^T(t)]\mathbf{Q}\begin{bmatrix}\tilde{\imath}(t)\\ \zeta(t)\end{bmatrix} + \tilde{\mathbf{u}}^T\mathbf{R}\tilde{\mathbf{u}}\,dt, \tag{14}$$

where $\mathbf{Q}$ and $\mathbf{R}$ are weighting matrices and ζ is an artificial state created to introduce integral action, which effectively corrects the effect of model mismatches, $\zeta = C_\zeta \int \tilde{\imath}\,dt$, where C_ζ is a weighting matrix.

4. Experimental results

The optimization is carried out over the time interval $t \in [t_0, t_F] = [0.4\,\mathrm{s}, t_F]$, where t_F is the time when the desired q profile and β_N value must be achieved and is employed as a design parameter. Two of the NBI (30L and 30R) are dedicated to Motional Stark Effect (MSE) diagnostics, which are used in the real time EFIT calculation to obtain measurements of the q profile [17], therefore they are not available for control. Due to lack of availability, the counter current NBIs are not considered either, therefore leaving four NBIs to be optimized in the feedforward control sequence, two on-axis NBIs (330L and 330R) and two off-axis NBIs (150L and 150R). Due to the difficulty in controlling the line averaged density, we choose not to optimize the density evolution and instead we prescribe it based on shots that had most closely achieved the target profiles.

The targets are all monotonically increasing q profiles with varying levels of q values at the plasma center and plasma edge. For the L-mode discharges we considered three different targets. The obtained q profile for each of the three targets are shown in Fig. 3. In Fig. 3, we show both the obtained q profile with feedforward (FF) control alone and combined feedforward and feedback (FF + FB) control at the best-matching time. In all cases, feedback control improves the obtained q-profile matching error significantly, even with varying initial conditions. Usually, the q profile with feedforward control alone falls to one before the target time regardless of the initial condition. This result is primarily due to slight modeling errors in the current diffusion rate, which lead to a nonsatisfactory feedforward control policy. This emphasizes the importance of feedback control, which is able to account for the modeling errors and to bring the q profile back as close as possible to the target. Similar results were obtained for H-mode shots as shown in Fig. 4. The control design process is nearly identical in both L-mode and H-mode discharges; the main differences are that the model parameters are adjusted appropriately for each case and the optimization constraints include minimum power limits to avoid the possibility of back transitions to L-mode.

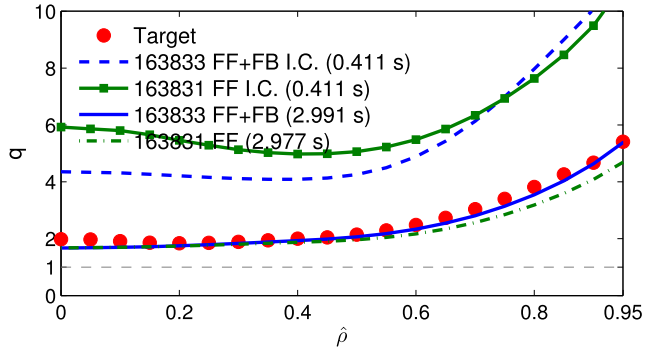

Fig. 4. Obtained q profiles during H-mode discharges. FF-only control (green) and FF + FB control (blue) profiles at the initial time and the desired target time ($t_F = 3.0$ s) are plotted. The red circles mark the target q profile. (For interpretation of the references to color in this figure legend, the reader is referred to the web version of the article.)

5. Conclusions

By combining feedforward optimization via nonlinear programming and linearized feedback control desired q profiles were attained in both L-mode and H-mode DIII-D discharges. While results are promising, they show the sensitivity of the feedforward control solution to model mismatches. Since this solution is computed offline, the feedforward design can however be improved by increasing the complexity of the model. Feedback control remains necessary due not only to the lack of a perfect model but also to the existence of plasma disturbances.

Acknowledgment

Work supported by the US DoE (DE-SC0010661).

References

[1] T.C. Luce, et al., Phys. Plasmas 11 (5) (2004) 2627–2636.
[2] G. Gormezano, et al., Nucl. Fusion 47 (2007) S285–S336.
[3] J. Ferron, et al., Phys. Plasmas 12 (2005) 056126.
[4] F. Hinton, et al., Rev. Mod. Phys. 48 (1976) 239–308.
[5] Y. Ou, et al., Fusion Eng. Des. 82 (2007) 1153–1160.
[6] J.E. Barton, et al., 52nd IEEE Conf. on Decision and Control, 2013.
[7] F.B. Argomedo, et al., Nucl. Fusion 53 (3) (2013) 033005.

[8] N.M. Trang, et al., 19th World Congress of the International Federation of Automatic Control, 2014, pp. 11398–11403.
[9] J.E. Barton, et al., Plasma Phys. Control. Fusion 57 (11) (2015) 115003.
[10] M.D. Boyer, et al., Plasma Phys. Control. Fusion 55 (10) (2013) 105007.
[11] Y. Ou, E. Schuster, et al., Control Eng. Pract. 19 (2011) 22–31.
[12] E. Maljaars, et al., Nucl. Fusion 55 (2) (2015) 023001.
[13] W. Wehner, et al., 54th IEEE Conf. on Decision and Control, 2015.
[14] J.T. Betts, J. Guid. Control Dyn. 21 (2) (1998) 193–207.
[15] J. Nocedal, S.J. Wright, Numerical Optimization, 2nd ed., Springer, Berlin, 2006.
[16] B. Sengupta, et al., NeuroImage 98 (2014) 521–527.
[17] J. Ferron, et al., Nucl. Fusion 38 (1998) 1055.